1-15-2000

Approximate Description of the Three Dimensional Director and Electric Field in a Liquid Crystal Display at a High Voltage

G. Panasyuk

David W. Allender
Kent State University - Kent Campus, dallende@kent.edu

Approximate description of the three dimensional director and electric field in a liquid crystal display at a high voltage

G. Panasyuk[a] and D. W. Allender
Liquid Crystal Institute and Department of Physics, Kent State University, Kent, Ohio 44242

(Received 3 August 1999; accepted for publication 13 October 1999)

An approximate analytical approach for describing properties of a liquid crystal display associated with a homeotropic to multidomainlike transition for a liquid crystal with a positive dielectric anisotropy was developed. The electrode and surface coating of the display are prepared in such a way that in the absence of an electric field (dark state) the liquid crystal alignment is homeotropic. The bright state corresponds to a situation when a high voltage is applied to the interdigitated electrodes located on both substrates, which causes a director deformation of a multidomain type. Approximate solutions for the three dimensional electric field and director configuration in the case of strong homeotropic anchoring were obtained to describe the bright state. It was found that two different defect structures are possible for the director configuration: one corresponds to a wall defect and the other to two disclination lines. A first order phase transition between the two structures is predicted at a particular value of the voltage. An estimate of this critical voltage is obtained. © *2000 American Institute of Physics.* [S0021-8979(00)04102-5]

I. INTRODUCTION

Liquid crystal displays (LCDs) represent a major technology in flat panel displays. Most of the LCDs produced today use twisted nematic (TN) or supertwisted nematic (STN) modes. The TN and STN displays show excellent electro-optic characteristics when the point of observation is close to normal to the screen but the quality of the displayed image decreases rapidly at oblique viewing angle. Various types of liquid crystal (LC) displays have been developed to improve the viewing angle quality and electro-optic properties of the TN and STN devices. Among them the in-plane switching (IPS),[1–4] the vertical alignment (VA),[5,6] the optically compensated bend,[7,8] the homogeneous-to-twisted planar,[9,10] and the dual-domainlike vertical alignment[11–13] modes have shown very good viewing angle characteristics. However, the single domain VA mode has intrinsic problems with brightness uniformity.[14,15] The IPS mode has an excellent contrast ratio at a wider range of viewing angles than the TN mode but the brightness and the color characteristics have a viewing angle dependence. Besides, the rubbing process required to obtain the necessary homogeneous alignment can introduce dust particles and cause electrostatic charges which may damage the thin film transistors in an active matrix display.

Recently two new rubbing-free types of LCDs were proposed. The first of these is a liquid crystal display mode which combines the concepts of IPS and VA.[16–18] This LCD uses a deformation transition from homeotropic alignment controlled by an in-plane electric field. It shows a very wide viewing angle when a negative birefringent compensation film is added.[18] The other LC device is associated with a homeotropic to multidomainlike (HMD) transition for a liquid crystal with a positive dielectric anisotropy ϵ_a. It has been experimentally investigated[19] and it has a wide viewing angle, excellent color characteristics, and a fast response time.[19]

A theoretical description of these types of LC cells is useful because it will enable the optimal conditions for their functioning to be determined. In particular, this article is devoted to modeling of the HMD cell. Figure 1 shows a schematic diagram of the cell. It is prepared in such a way that in the absence of an electric field (dark state) the liquid crystal alignment is vertical, or homeotropic. The bright state corresponds to the situation when a voltage larger than about 10 V is applied to the interdigitated electrodes located on both substrates. Our theoretical model assumes the electrodes to be infinitely thin. This causes nonanalyticity in the electric potential, because all its spatial derivatives, in particular, the electric field, diverge along the sharp edges of the electrodes. It causes difficulties in the numerical solution of the problem, so we developed an analytical approach to describe approximately the bright state of the cell.

II. GENERAL IDEAS OF THE DESCRIPTION

The schematic diagram of the cell is pictured in Fig. 2. We chose the coordinate system as in the picture, assuming that the electrode planes have coordinates $z=\pm d/2$ ($+d/2$ for the top plane). The + and − electrodes have potentials $+u/2$ and $-u/2$, respectively.

It can be seen from the picture that the system possesses the following symmetries: (1) 2L periodicity along both the x and y directions for any variables; (2) mirror symmetry with respect to the vertical planes at $x=\pm L/2,\ \pm 3L/2,\ldots$ and $y=\pm L/2,\ \pm 3L/2,\ldots$, [this ensures that the electric potential Φ satisfies the relation

$$\partial_x \Phi(x,y,z)=\partial_y \Phi(x,y,z)=0 \tag{1}$$

[a]Electronic mail: georgy@columbo.kent.edu

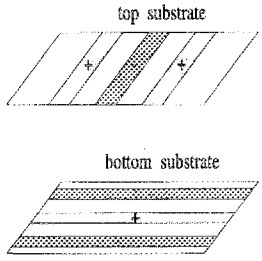

FIG. 1. A schematic diagram of the LC cell structure with interdigitated electrodes.

at the position of the mirror symmetry planes], and (3) "twisted symmetry," where, for example,

$$\Phi(x,y,z)=\Phi(y,x,-z). \tag{2}$$

Due to the last property, it is sufficient to consider only the upper ($z\geq 0$) region.

It was found also that the system possesses a defect structure. Each defect is essentially a twist wall. In particular, when the voltage is not too high there are wall defects[20] which go approximately along the vertical diagonal planes. At every point of such a plane the electric field $\mathbf{E}$ is perpendicular to the initial (homeotropic) director alignment and the torque due to the electric field on the director is zero. The director rotates by nearly π when one moves through the plane along any line perpendicular to it. This causes the defect structure which will be described later in this section and in Sec. IV.

Assuming strong boundary conditions for the director $\mathbf{n}(\mathbf{r})$, we can approximately divide the slab into three main parts:

(1) the near-electrode layer of thickness Δ (see Fig. 3)
(2) the wall region,
(3) the remaining, "bulk" part.

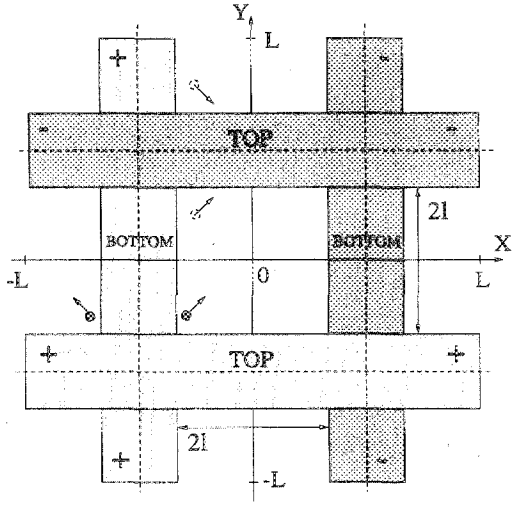

FIG. 2. Top view of the cell showing the periodicity and coordinate system of the display. Planes of the mirror symmetry are shown as dashed lines.

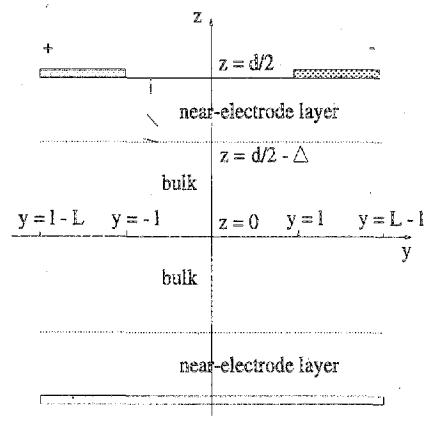

FIG. 3. Side view of the cell showing the near-electrode layer and relaxation of the director to its bulk distribution across the layer.

In our approach the wall region consists of a vertical plane with homeotropic alignment at the center of the wall and an adjacent vertical layer to each side where the director field twists to fit its distribution in the bulk.

Introducing the elastic (F_d) and field (F_f) free energy densities, we can express the whole free energy F in the form:

$$\mathrm{F}=\int d\rho\int_0^{d/2}dz(F_d+F_f)-\frac{1}{8\pi}\int d\rho\int_{d/2}^{\infty}dzE^2, \tag{3}$$

where, with usual notations,[20]

$$F_d=\frac{K_1}{2}(\nabla\cdot\mathbf{n})^2+\frac{K_2}{2}[\mathbf{n}\cdot(\nabla\times\mathbf{n})]^2+\frac{K_3}{2}[\mathbf{n}\times(\nabla\times\mathbf{n})]^2, \tag{4}$$

and

$$F_f=-\frac{\epsilon_a}{8\pi}(\mathbf{n}\cdot\mathbf{E})^2-\frac{\epsilon_\perp}{8\pi}E^2,\quad \epsilon_a=\epsilon_\parallel-\epsilon_\perp. \tag{5}$$

Due to the $2L$ periodicity, the x and y integration can be restricted to one periodic cell

$$\int d\rho\equiv\int_{-L}^{L}dx\int_{-L}^{L}dy \tag{6}$$

and we have to introduce the vacuum electric energy term in Eq. (3) because the electric field is not localized inside the slab.

It can be assumed that in the bulk of the slab the scale of spatial variations of $\mathbf{n}(\mathbf{r})$ is the same as for the electric potential. In this case, as can be seen from Eqs. (4) and (5), the characteristic value of the ratio F_d/F_f is determined by the parameter

$$\delta=\frac{4\pi K_m}{\epsilon_a(u)^2}, \tag{7}$$

where K_m is the maximum value of the elastic constants. To obtain an estimate of δ, we use the experimental value of 7.4 for ϵ_a at 20° and 1 kHz[19] and a typical value of 1.5×10^{-6} dyn for K_m. Then, if $u\geq 10$ V, $\delta\leq 0.004$. After obtaining the analytical solution for $\mathbf{n}(\mathbf{r})$, we were able to confirm the above-mentioned assumption directly. On the other hand,

$\mathbf{n}(\mathbf{r})$ changes rapidly across the near electrode or wall layers and we cannot neglect completely the elastic energy in those regions. The thicknesses Δ and Δ_w of the near electrode and wall layers are of order of the electric relaxation length and can be represented as $l_c\delta^{1/2}$, where l_c is a characteristic size of the cell; $l_c \propto l$ (see Figs. 2 and 3) and is of order of 10 μm in the experiment.[19] Particular expressions for Δ and Δ_w will be introduced later.

A. In the bulk

Taking into account the condition $\mathbf{n}^2=1$ and neglecting the elastic energy completely, the Euler-Lagrange equations in the bulk can be written in the simple form:

$$-\frac{\epsilon_a}{4\pi}(\mathbf{n}\cdot\mathbf{E})\mathbf{E}=\lambda\mathbf{n}, \tag{8}$$

$$\nabla[\epsilon_\perp\mathbf{E}+\epsilon_a(\mathbf{n}\cdot\mathbf{E})\mathbf{n}]=0. \tag{9}$$

Equation (8) can be solved to obtain the following relationship between $\mathbf{n}$ and $\mathbf{E}$:

$$\mathbf{n}=\frac{\mathbf{E}}{E}, \quad E=|\mathbf{E}|, \quad \lambda=-\frac{\epsilon_a E^2}{4\pi}. \tag{10}$$

Substituting Eq. (10) into (9), we can write eventually the equation for the electric potential

$$\nabla(\epsilon_\parallel\mathbf{E})=0, \quad \text{or} \quad \nabla^2\Phi=0, \tag{11}$$

assuming that $\epsilon_\parallel$ and $\epsilon_\perp$ do not depend on $\mathbf{r}$.

In the case when the voltage is so high that even $\delta^{1/2}$ is negligibly small, the bulk equations hold everywhere in the slab. The corresponding solution $\mathbf{n}\equiv\mathbf{n}_0=\mathbf{E}/E$, $\mathbf{E}\equiv\mathbf{E}_0=-\nabla\Phi_0$ for this zero order approximation can be found by solving the Laplace equation

$$\nabla^2\Phi_0=0 \tag{12}$$

with the following conditions on the electric field:

$$\Phi_0(\mathbf{r})=\pm\frac{u}{2} \quad \text{on the electrodes,}$$

and

$$E_0(\mathbf{r})\to 0 \quad \text{when} \quad |z|\to\infty. \tag{13}$$

B. In the near-electrode layer

In a more realistic case when $\delta^{1/2}$ is small but not negligible, the near-electrode layer must be taken into account, and the director distribution in it can be found in the following way. At first, we can split F_d in Eq. (4) into three parts: $F_d=F_{d1}+F_{d2}+F_{d3}$, where F_{d1} contains only z derivatives, F_{d3} contains only x and y derivatives, and F_{d2} contains mixed derivatives, i.e., x and z or y and z. It is obvious that

$$\begin{aligned} F_{d1}&\propto O(K_m/\Delta^2)=O(K_m/l_c{}^2\delta)\\ &=O(K_m\epsilon_a l_c{}^2E^2/4\pi K_m l_c{}^2)\\ &=O(\epsilon_a E^2/4\pi). \end{aligned} \tag{14}$$

Thus, the F_{d1} term cannot be neglected. On the other hand

$$\begin{aligned} F_{d2}&\propto O(K_m/l_c\xi)=O(K_m/l_c{}^2\delta^{1/2})\\ &=\delta^{1/2}O(K_m/l_c{}^2\delta)\\ &=\delta^{1/2}O(\epsilon_a E^2/4\pi), \end{aligned} \tag{15}$$

$$F_{d3}\propto O(K_m/l_c{}^2)=\delta O(\epsilon_a E^2/4\pi) \tag{16}$$

so that the terms F_{d2} and F_{d3} are reduced by at least a factor of $\delta^{1/2}$ compared to F_{d1}, which is of order of the electric field energy density.

Using the Maxwell equation

$$\nabla\times\mathbf{E}=0 \tag{17}$$

and neglecting x and y derivatives again, it can be found that $E_{x,y}$ do not depend on the z coordinate. Due to this property, we can neglect $d\phi/dz$ in F_{d1} (ϕ is an azimuthal angle). Because the field $\mathbf{E}$ in the bulk is $\mathbf{E}=\mathbf{E}_0[1+O(\delta^{1/2})]$ and the perturbation source is the small thickness of the layer, we can use $\mathbf{E}\approx\mathbf{E}_0$ on the border with the bulk as a boundary condition for the subsequent determination of $\mathbf{E}$ and $\mathbf{n}$ in the layer. In particular, we can write down that

$$\begin{aligned} E_x(x,y,z)&=E_{0x}(x,y,d/2-\Delta),\\ E_y(x,y,z)&=E_{0y}(x,y,d/2-\Delta), \end{aligned} \tag{18}$$

where $\mathbf{E}_0(x,y,d/2-\Delta)$ is the electric field in the zero order approximation on the border between the layer and bulk. The same ideas are also correct for the description of the wall layer.

Introducing the director field in the form $\hat{\mathbf{n}}=(\hat{\mathbf{x}}\cos\phi_0+\hat{\mathbf{y}}\sin\phi_0)\sin\theta+\hat{\mathbf{z}}\cos\theta$, where $\hat{\mathbf{x}}$, $\hat{\mathbf{y}}$, and $\hat{\mathbf{z}}$ are the unit vectors along the x, y, and z axes, we can say that $\phi_0=\phi_0(x,y,d/2-\Delta)$ is determined by the electric field on the border in the zero approximation and the free energy functional in the layer takes the simple form:

$$\mathrm{F}_l=\int d\rho\int_{d/2-\Delta}^{d/2}dz\left\{\frac{1}{2}(K_1\sin^2\theta+K_3\cos^2\theta)\left[\frac{d\theta}{dz}\right]^2-\frac{\epsilon_\perp}{8\pi}E^2-\frac{\epsilon_a}{8\pi}(\mathbf{n}\cdot\mathbf{E})^2\right\}. \tag{19}$$

The corresponding Euler-Lagrange equations are:

$$(K_1\sin^2\theta+K_3\cos^2\theta)\frac{d^2\theta}{dz^2}-(K_3-K_1)\sin\theta\cos\theta\left[\frac{d\theta}{dz}\right]^2+\frac{\epsilon_a}{4\pi}(\mathbf{n}\cdot\mathbf{E})(E_{0\rho}\cos\theta-E_z\sin\theta)=0, \tag{20}$$

$$\partial_z[\epsilon_\perp E_z+\epsilon_a(\mathbf{n}\cdot\mathbf{E})\cos\theta]=0, \tag{21}$$

where

$$(\mathbf{n}\cdot\mathbf{E})=E_z\cos\theta+E_{0\rho}\sin\theta, \quad E_{0\rho}\equiv|\mathbf{E}_{0\rho}| \tag{22}$$

and $\mathbf{E}_{0\rho}=\hat{\mathbf{x}}E_{0x}+\hat{\mathbf{y}}E_{0y}$ does not depend on z across the layer. Using the above mentioned condition $\mathbf{E}\approx\mathbf{E}_0$ on the layer border, one can easily obtain the expression for E_z inside the layer

$$E_z=\frac{\epsilon_\parallel E_{0z}-\epsilon_a E_{0\rho}\sin\theta\cos\theta}{\epsilon_\perp+\epsilon_a\cos^2\theta}. \tag{23}$$

Substituting E_z into Eq. (20) and solving the resulting equation with the boundary conditions

$$\theta(d/2)=0, \quad \theta(d/2-\Delta)\equiv\theta_0=\arcsin(E_{0\rho}/E_0) \tag{24}$$

one can determine the director distribution across the layer.

The following ideas allow us to define the value of Δ and simplify to some extent the layer description. It follows from the solution of the boundary problem (see the next section), that the electric field distribution is close to planar in any inner square where $-l<x,y<l$ (see Figs. 2 and 3) and z is some fixed number between $-d/2+\Delta$ and $d/2-\Delta$. Therefore $|E_{0z}|\ll|E_{0\rho}|$. Characteristic values of $E_{0\rho}/u\approx E_0/u$ lie between 0.04 and 0.06 μm^{-1} and $70°<\theta_0(x,y)\leqslant 90°$. This means that the director distribution relaxes from homeotropic at the electrode plane to essentially planar at the border. Strictly speaking, we have to solve Eq. (20) on the interval $[0,\Delta(x,y)]$ along the z coordinate with the boundary conditions (24) at every point (x,y). However, as was already mentioned, the scale of spatial variation of $E_{0\rho}\approx E_0$ is $l_c\propto 10\ \mu m$. This means that relative changes of $E_{0\rho}$ in a distance $\Delta z=\xi_3\equiv(4\pi K_3/\epsilon_a E_{0\rho}^2)^{1/2}$ are about 5% ($\xi_3\approx 0.4\ \mu m$ at $K_3=1.5\times10^{-6}$ dyn and $u=20$ V). Besides, the relative deviation of $E_{0\rho}$ from its average value $\bar{E}_{0\rho}$ when x and y vary across the inner square do not exceed 20%. This fact provides the reason for the introduction of the relaxation length and allows us to consider the border as a plane perpendicular to the z coordinate at $z=d/2-\Delta$ with

$$\Delta=n_l\bar{\xi}_3\equiv n_l\xi_3(\bar{E}_{0\rho})\approx n_l\xi_3(\bar{E}_0), \tag{25}$$

where n_l is a number of order one and $\bar{E}_{0\rho}$ and $\bar{E}_0$ are averaged values of the electric field along the border. In order to estimate a value of Δ, approximate Eq. (22) by $\mathbf{n}\cdot\mathbf{E}\approx E_{0\rho}\sin\theta$, where $E_{0\rho}$ is constant along the z coordinate, and substitute it in Eq. (19). Assuming that at infinite distance from the electrode plane θ takes a value θ_0 which is equal to the bulk angle at the layer border in Eq. (24), one finds

$$n_l=\int_0^{\theta_{01}} dx\left(\frac{K_{13}\sin^2 x+\cos^2 x}{\sin^2\theta_0-\sin^2 x}\right)^{1/2}, \quad K_{13}=K_1/K_3, \tag{26}$$

by solving the corresponding Euler-Lagrange equation. In this relation $\theta_{01}=\theta(\Delta)$ is the value of the solution $\theta(z)$ of the simplified Euler-Lagrange equation at the border. If we take into account that $0.5\leqslant K_{13}\leqslant 1$ and demand that $\theta_{01}\approx 0.9\theta_0$ it is easy to find that $n_l\approx 2$. In such a case relative changes of $E_{0\rho}$ through the layer are only about 10%.

On the other hand in the regions under or above the electrodes (and close to them) the director distribution is already close to homeotropic, because the electric field is perpendicular to the electrode stripes. In such a situation it is not very important how to choose Δ in those regions, and it is possible to spread the border plane defined by Eq. (25) to the entire region of periodicity.

Analysis of numerical solutions of Eq. (20) for a wide range of the boundary conditions (24) showed that the solution $\theta(z)$ is a smooth monotonic function close to

$$\theta(z)\approx(d/2-z)\theta_0/\Delta. \tag{27}$$

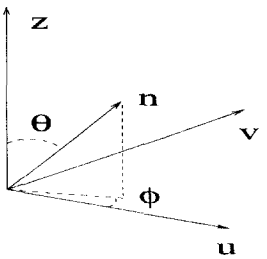

FIG. 4. A coordinate system describing the director distribution inside the wall layer, where the v coordinate is counted from a point on the central plane $y=x$.

C. In the wall layer

In this region the main ideas of the description are essentially the same. If we introduce a coordinate system (u,v,z) produced by rotating the x-y system by 45° around the z-axis counterclockwise, so that $\hat{\mathbf{v}}$ is perpendicular to the wall plane and $\hat{\mathbf{u}}$ is along the diagonal of an inner square, only v derivatives must be taken into account. Define the director inside the wall layer as $\hat{\mathbf{n}}=\hat{\mathbf{z}}\cos\theta+\sin\theta(\hat{\mathbf{u}}\cos\phi+\hat{\mathbf{v}}\sin\phi)$ (see Fig. 4). Again, using Eq. (17) one can find that the electric field components

$$E_u=E_{0u}(u,\Delta_w,z), \quad E_z=E_{0z}(u,\Delta_w,z) \tag{28}$$

do not change along the v coordinate within the wall, taking their values on the border between the wall layer and bulk. Then, analysis of the solution of the boundary problem shows that in the absence of the wall defect $\mathbf{E}_0$ and $\mathbf{n}_0=\mathbf{E}_0/E_0$ change smoothly along any line crossing the central diagonal plane, staying approximately parallel to the diagonal of the inner square in a horizontal plane. That means that $E_{0v}=E_{0v}(u,\Delta_w,z)$ and the angle

$$\phi_0=\arccos(E_{0u}/E_{0\rho}), \quad E_{0\rho}=(E_{0u}^2+E_{0v}^2)^{1/2} \tag{29}$$

on the wall layer border are relatively small. In the case of the wall defect θ changes from 0 at $v=0$ to

$$\theta_0=\arcsin(E_{0\rho}/E_0) \tag{30}$$

at $z=\Delta_0$, where θ_0 is close to $\pi/2$, because $E_{0\rho}\approx E_{0u}\approx E_0$. On the other hand, only small variations in ϕ are possible across the layer. This is because $E_u=E_{0u}$ is constant and E_v is relatively small, so there is no reason for any significant changes of the orientation of the director component lying in the (u,v) plane. Thus, it is possible to put $\phi\approx\phi_0$ in the above expression for $\hat{\mathbf{n}}$ in the wall layer and to write down the following expression for the free energy density inside the layer:

$$F_w=\frac{1}{2}\left[\frac{d\theta}{dv}\right]^2[K_2\cos^2\phi_0+\sin^2\phi_0(K_1\cos^2\theta+K_3\sin^2\theta)]$$
$$-\frac{\epsilon_\perp}{8\pi}E^2-\frac{\epsilon_a}{8\pi}(\mathbf{n}\cdot\mathbf{E})^2, \tag{31}$$

where

$$\mathbf{n}\cdot\mathbf{E}=E_{0z}\cos\theta+\sin\theta(E_{0u}\cos\phi_0+E_v\sin\phi_0). \tag{32}$$

The corresponding Euler-Lagrange equations are

$$[K_2\cos^2\phi_0+\sin^2\phi_0(K_1\sin^2\theta+K_3\cos^2\theta)]\frac{d^2\theta}{dv^2}$$
$$+(K_3-K_1)\sin^2\phi_0\sin\theta\cos\theta\left[\frac{d\theta}{dv}\right]^2+\frac{\epsilon_a}{4\pi}(\mathbf{n}\cdot\mathbf{E})$$
$$\times[(E_{0u}\cos\phi_0+E_v\sin\phi_0)\cos\theta-E_z\sin\theta]=0, \quad (33)$$

$$\partial_v[\epsilon_\perp E_v+\epsilon_a(\mathbf{n}\cdot\mathbf{E})\sin\theta\sin\phi_0]=0, \quad (34)$$

and from Eq. (34) one can express the v component of the electric field, using the boundary condition $\mathbf{E}\approx\mathbf{E}_0$ on the wall layer border

$$E_v=\frac{\epsilon_\parallel E_{v0}-\epsilon_a(E_{0z}\cos\theta+E_{0u}\sin\theta\cos\phi_0)\sin\theta\sin\phi_0}{\epsilon_\perp+\epsilon_a\cos^2\theta\sin^2\phi_0}, \quad (35)$$

where E_{0z} and E_{0u} are determined from Eq. (28). Substituting E_v into Eq. (33) and solving the resulting equation with the boundary conditions

$$\theta(0)=0, \quad \theta(\Delta_w)\equiv\theta_0=\arcsin(E_{0\rho}/E_0), \quad (36)$$

one can determine the director distribution across the wall layer.

Equation (33) can be simplified to estimate the thickness Δ_w. Using the smallness of E_{0z}/E_{0u}, E_v/E_{0u}, and ϕ_0, Eq. (33) gives approximately

$$\frac{d^2\theta}{dv^2}+\frac{1}{\xi_2^2}\sin\theta\cos\theta=0, \quad \xi_2=\left(\frac{4\pi K_2}{\epsilon_a E_{0u}^2}\right)^{1/2}. \quad (37)$$

It is worth noting that the director bends and splays in the near-electrode layer but in contrast it primarily twists in the wall layer.

In the case when ξ_2 does not depend on spatial variables, the exact solution of Eq. (37) describes relaxation of the director to its distribution controlled by the electric field E_{0u}. In our case, when ξ_2 depends on $\mathbf{r}$, it is reasonable again, as in the case of the near-electrode layer, to choose Δ_w as a compromise between the two competing factors. On the one hand, one has to choose Δ_w large enough for the director to relax to its bulk distribution at $v=\Delta_w$ as close as possible. On the other hand Δ_w must be much smaller than a characteristic size of the cell l_c which is the scale of spatial variations of $\mathbf{E}_0$ or $\mathbf{n}_0$. Otherwise one has to take into account in Eq. (37) these spatial variations, and u and z derivatives in the elastic energy would be comparable with v derivatives. Thus, taking all the above mentioned considerations into account, it is possible to admit the following estimate for the wall layer thickness:

$$\Delta_w=n_w\xi_2, \quad \xi_2=\left(\frac{4\pi K_2}{\epsilon_a\bar{E}_{0u}^2}\right)^{1/2}, \quad (38)$$

where $\bar{E}_{0u}$ is the averaged value of E_{0u} along the wall layer border plane as in the case of the near-electrode layer, and for estimating a number n_w we can use Eq. (26) with $K_{13}=1$. Because K_2 is smaller than K_3 (usually K_3/K_2 is between 3 and 4), $n_w\approx 2.5$ for the case when $\theta_{01}=0.95=\theta_0$. This choice provides even smaller (about 5%) relative changes of the electric field across the wall layer than in the case of the near-electrode layer.

III. SOLUTION OF THE BOUNDARY PROBLEM

The general form of the solution of the Laplace equation is

$$\Phi_{LC}(\mathbf{r})=\sum_{p=0,q=0}^{\infty}[(\alpha_{pq}\cosh(d_{pq}\bar{z})-\beta_{pq}\sinh(d_{pq}\bar{z})]$$
$$\times\cos(2\pi q\bar{y})\sin[(2p+1)\pi\bar{x}]$$
$$+[\alpha_{pq}\cosh(d_{pq}\bar{z})+\beta_{pq}\sinh(d_{pq}\bar{z})]$$
$$\times\cos(2\pi q\bar{x})\sin[(2p+1)\pi\bar{y}] \quad (39)$$

in the slab, where $\bar{x}=x/L$, $\bar{y}=y/L$ and $\bar{z}=2z/d$, and

$$\Phi_{vac}(\mathbf{r})=\sum_{p=0,q=0}^{\infty}\{\alpha_{pq}^v\cos(2\pi q\bar{y})\sin[(2p+1)\pi\bar{x}]$$
$$+\beta_{pq}^v\cos(2\pi q\bar{x})\sin[(2p+1)\pi\bar{y}]\}$$
$$\times\exp(-d_{pq}|\bar{z}|) \quad (40)$$

in the vacuum, where

$$d_{pq}=\frac{\pi d}{2L}[(2p+1)^2+4q^2]^{1/2}. \quad (41)$$

To determine the coefficients α and β, we introduce the electrode plane potential $V(x,y)$ which satisfies the following conditions. It is a continuous and $2L$-periodic function of x and y, has the value $\pm u/2$ on the electrodes, and satisfies the symmetry relation:

$$V(x,y)=V(x,L-y). \quad (42)$$

Using these conditions, $V(x,y)$ on the interval $-l\leq y\leq l$ may be written as

$$V(x,y)/u=-\frac{y}{2l}+\Delta V(x,y), \quad (43)$$

where

$$\Delta V(x,y)=\sum_{m=1,q=0}^{\infty}\sin[\pi m(\bar{y}+\bar{l})/2\bar{l}]\{f_{mq}\cos(2\pi q\bar{x})$$
$$+g_{mq}\sin[(2q+1)\pi\bar{x}]\}, \quad \bar{l}=l/L. \quad (44)$$

The number of f and g coefficients in the complete solution is of course infinite but an approximate solution may be found by truncating the series. It is convenient then to unite the coefficients f_{mq} and g_{mq} in the expression for $\Delta V(x,y)$ into a vector

$$(\{f_{mq}\},\{g_{mq}\})\equiv\mathbf{f}_N, \quad (45)$$

where N is the number of coefficients kept in a given truncation approximation. Using the properties of $2L$ periodicity and continuity of the potential across the border between the liquid crystal slab and the vacuum, we can rearrange $V(x,y)$ in terms of $\sin[(2p+1)\pi\bar{y}]$, $\cos(2\pi q\bar{y})$ and express the α and β coefficients in Φ_{LC} and Φ_{vac} in terms of $\mathbf{f}_N$. To obtain $\mathbf{f}_N$,

the variational principle may be used to minimize the electric free energy F_f. Because Φ_{LC} and Φ_{vac} satisfy the Laplace equation, we can rewrite F_f as the electrode plane functional

$$F_f=\frac{1}{8\pi}\int d\rho(\Phi_{vac}\partial_z\Phi_{vac}-\epsilon_\parallel\Phi_{LC}\partial_z\Phi_{LC}). \tag{46}$$

Substituting here Eqs. (39) and (40) and integrating the resulting expression explicitly, we represent F_f as the quadratic form with respect to the arbitrary coefficients f_{mq} and g_{mq}. After that, differentiating F_f with respect to these coefficients and equating the results to zero, we will get the following system of linear inhomogeneous algebraic equations with respect to f_{mq} and g_{mq}:

$$\sum_{n=1}^{n_f} w_{m0n}f_{n0}+\frac{1}{2}\sum_{p=0}^{n_g} v_{m0np}g_{np}=r_m,\quad m=1,2,\ldots n_f, \tag{47}$$

$$\sum_{n=1}^{n_f} w_{mrn}f_{nr}+\sum_{n,p=0}^{n_g} v_{mrnp}g_{np}=0,\quad r,\ m=1,2,\ldots n_f, \tag{48}$$

$$\sum_{n=1}^{n_f} t_{mrn0}f_{n0}+\sum_{n,q=1}^{n_f} t_{mrnq}f_{nq}+\sum_{p=0}^{n_g} z_{mrn}g_{nr}=s_{mr},\quad r,\ m=0,1,\ldots n_g. \tag{49}$$

The coefficients in Eqs. (47)–(49) are determined by the following formulas:

$$w_{mrn}=\sum_{n=0}^{\infty} b_{np}D_{mpr},\quad v_{mrnp}=2b_{mp}G_{npr},$$

$$r_m=-\sum_{n=0}^{\infty} A_pD_{mp0},\quad t_{mrnq}=b_{nr}G_{mrq},$$

$$z_{mrn}=\frac{1}{4}F_{mrn0}+\frac{1}{2}\sum_{q=1}^{\infty} F_{mrnq},\quad s_{mr}=-A_rG_{mr0},$$

where

$$D_{mpr}=b_{mp}B_{pr},\quad F_{mrnq}=a_{nq}a_{mq}B_{rq},$$

$$B_{pr}=d_{pr}[2+\epsilon_\parallel(\tanh d_{pr}+\coth d_{pr})],$$

$$G_{mrq}=\frac{1}{2}d_{rq}a_{mq}\epsilon_\parallel(\tanh d_{pr}-\coth d_{pr}).$$

In the last formulas

$$A_p=-\frac{2\sin[(2p+1)\pi\bar{l}]}{\bar{l}\pi^2(2p+1)^2} \tag{50}$$

is a Fourier coefficient of a function

$$S_0(y)=\sum_{p=0}^{\infty} A_p\sin[(2p+1)\pi\bar{y}] \tag{51}$$

which is defined on the whole periodicity interval $(-L,L)$ in accordance to the following rules: $S_0(y)=-\bar{y}/2$ when $0\leqslant\bar{y}\leqslant\bar{l}$, $S_0(y)=-1/2$, if $\bar{l}\leqslant\bar{y}\leqslant 1-\bar{l}$ (along the "−" electrode), $S_0(y)=-(1-\bar{y})/2$, when $1-\bar{l}\leqslant\bar{y}\leqslant 1$ [due to Eq. (42)] and $S_0(y)=-S_0(-y)$ when $-1\leqslant\bar{y}\leqslant 0$. In addition,

$$a_{nq}=[1/(2n+1-4\bar{l}q)+1/(2n+1+4\bar{l}q)]\frac{4\bar{l}}{\pi}\cos(2\pi q\bar{l}),$$

$$b_{np}=[1/[(2p+1)\bar{l}-n]-1/[(2p+1)\bar{l}+n]]\frac{2\bar{l}}{\pi}\times\sin[(2p+1)\pi\bar{l}]$$

are the Fourier coefficients of functions $S_k(y)$, $k=1,2,3,\ldots$ where

$$S_{2n+1}(y)=\frac{1}{2}a_{n0}+\sum_{q=1}^{\infty} a_{nq}\cos(2\pi q\bar{y})\text{ for }n=0,1,2,\ldots, \tag{52}$$

and

$$S_{2n}(y)=\sum_{p=0}^{\infty} b_{np}\sin[(2p+1)\pi\bar{y}]\quad\text{for } n=1,2,3,\ldots. \tag{53}$$

Again, all the functions $S_k(y)$ can be described by the following relations: $S_k(y)=\sin[\pi k(\bar{y}+\bar{l})/2\bar{l}]$, when $0\leqslant\bar{y}\leqslant\bar{l}$, $S_k(y)=0$, if $\bar{l}\leqslant\bar{y}\leqslant 1-\bar{l}$, $S_k(y)=\sin[\pi k(1-\bar{y}+\bar{l})/2\bar{l}]$, when $1-\bar{l}\leqslant\bar{y}\leqslant 1$ and $S_k(y)=(-1)^{k+1}S_k(-y)$, if $-1\leqslant\bar{y}\leqslant 0$. Actually, the functions $S_k(y)$ determined by Eqs. (51)–(53) and the Fourier coefficients A_p, a_{nq}, and b_{np} come from the definitions of Eqs. (43) and (44) of the electrode plane potential $V(x,y)$ and its rearrangement in terms of $\sin[\pi(2p+1)\bar{y}]$ and $\cos(2\pi q\bar{y})$. The number N defined by Eq. (45) can be connected with the numbers n_f and n_g introduced in Eqs. (47)–(49) by the following relation: $N=n_f(n_f+1)+(n_g+1)^2$.

The system of Eqs. (47)–(49) can be represented in the compact form

$$\hat{M}\cdot\mathbf{f}_N=\mathbf{R} \tag{54}$$

with the known matrix $\hat{M}$ and vector $\mathbf{R}$ determined by the system. This equation is satisfied by a unique vector $\mathbf{f}_N$ which determines the desired distributions $\Phi_{LC}\equiv\Phi_0$, $\mathbf{E}_0$, and $\mathbf{n}_0$.

We make an important observation about the system of Eq. (54). It becomes inconvenient to solve Eq. (54) exactly when $N\geqslant 50$. On the other hand, as will be explained later, an accurate description of the director distribution requires $N\geqslant 700$. Fortunately, the matrix $\hat{M}$ can be represented as $\hat{M}_0+\Delta\hat{M}$, where $\hat{M}_0$ is diagonal and $\Delta\hat{M}$ is small with respect to $\hat{M}_0$. Thus, we can solve Eq. (54) by means of an iterative procedure

$$\mathbf{f}_N^{(n)}=\hat{M}_0^{-1}(\mathbf{R}-\Delta\hat{M}\mathbf{f}_N^{(n-1)}) \tag{55}$$

for $n\geqslant 1$, which has rapid convergence for any reasonable N.

IV. RESULTS AND DISCUSSION

As was mentioned above, a large number of coefficients f_{mq} and g_{mq} is needed for a proper description of the system.

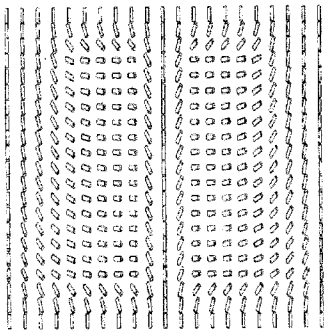

FIG. 5. Director distribution in the vertical y-z plane at $x=0$ for the case of the wall defect.

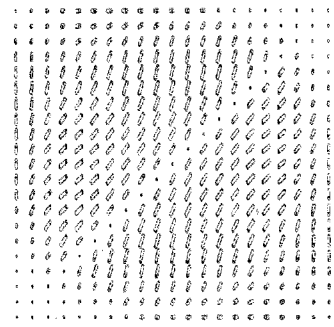

FIG. 6. Director distribution in the horizontal x-y plane at $z=0.1d$ for the case of the wall defect.

The reason for this is nonanalyticity of the electric potential $V(\mathbf{r})$ near the sharp edges of the electrodes.[21] In our case $V(\mathbf{r})$ behaves as

$$V(\mathbf{r}) \approx \pm u/2 + C_1 |\Delta \mathbf{r}|^{1/2} \tag{56}$$

with the distance $|\Delta \mathbf{r}|$ from the straight lines described by the equations $y=\pm l$, $\pm(L-l)$, $\pm[2L+(L-l)]$,..., for $z=d/2$ and any x, and by the same equations with interchanging x and y at $z=-d/2$. In Eq. (56) C_1 is a constant which depends on the way an edge is approached.[21] Thus, all space derivatives of the potential, in particular the electric field $\mathbf{E}$, diverge along these lines. The property of Eq. (56) leads to a slow decay rate of the coefficients f_{mq} and g_{mq}, namely

$$f_{mq} \approx S_f(q)/m^{3/2}, \quad g_{mq} \approx S_g(q)/m^{3/2} \tag{57}$$

with respect to index m for large m. On the other hand, our study shows that f_{mq} and g_{mq} diminish very rapidly as q increases, and f_{mq} and g_{mq} with $q \geqslant 10$ may be neglected. Because of Eq. (57), it is mandatory to take into consideration all the coefficients f_{mq}, g_{mq} with $m \leqslant 50$, which gives their total number $N \propto 1000$. This is a consequence of the nonanalytical structure of the electric field. On the other hand, if we increase N to 3000, the result is practically the same as for $N=750$ (within 1% accuracy). This means that the described method is a practical way to solve the boundary problem.

Another interesting question is connected with the defect structure. Our theoretical study shows that an alternative to the wall defect is two disclination lines with strengths $m=\pm 1/2$ near the top and bottom substrates. In accordance with a simple estimate,[20] the energy of the wall defect (per unit area) is

$$W_w \approx \frac{2K_2}{\xi_2}, \tag{58}$$

where ξ_2 is determined by Eq. (38). When the voltage is not very high, W_w is relatively low and we have a characteristic director configuration with the wall defect pictured in Figs. 5 and 6. These two pictures illustrate the director distribution calculated in accordance to the scheme presented here for the following set of physical parameters: $K_1=0.7$, $K_2=0.4$, $K_3=1.5$ (in units of 10^{-6} dyn), $\epsilon_\parallel=19.4$, $\epsilon_\perp=12$, $l=10\,\mu$m, $d=5\,\mu$m, $L=30\,\mu$m, $u=14$ V. Figures 7(a) and 7(b) is taken from Fig. 2 of Ref. 19 and shows the experimental light transmission through the cell for two different orientations of the crossed polarizers. Black horizontal and vertical stripes correspond to the opaque electrodes used in Ref. 19. The observed dark diagonal lines can be interpreted as the presence of the wall defect in Fig. 6, where the director alignment stays homeotropic even in the presence of the electric field, as was already explained in Sec. II (see also Refs. 19 and 20). It can also be seen from Fig. 6, that the director in the inner square is aligned approximately along the diagonal. This explains the dark inner region in Fig. 7(a). In this case the angle between the analyzer A and horizontal electrodes is 45°, and the director is approximately oriented along either polarizer, or analyzer. When that angle is 0, there is a maximum in the light transmission [Fig. 7(b)].

Energy W_w increases with voltage, and for rather high electric field the wall may be replaced by two disclination lines which go inside the near-electrode layers approximately along the diagonal. The corresponding director configuration is illustrated by Figs. 8 and 9. In Fig. 9 a disclination line (which is not shown on the picture) goes through points on the inner square situated between cylinders rotated in the opposite directions.

The energy of the disclination lines (per unit length) can be estimated[20,22] as

$$W_l = 2 \cdot \pi m^2 K \left(\log \frac{R}{r_c} + \alpha \right) + 2 \cdot \frac{2K_2 \Delta}{\xi_2}. \tag{59}$$

In this formula $\pi m^2 K \log(R/r_c)$ is the macroscopic energy of elastic deformation associated with one line. It is derived in the one elastic constant approximation.[20] A characteristic

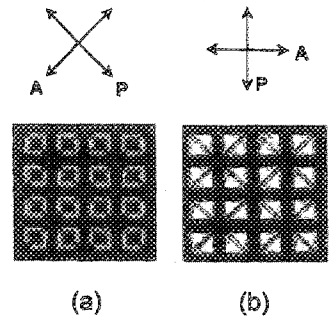

FIG. 7. The experimental transmission pattern with crossed polarizers at $u=14$ V (Ref. 19) when (a): the angle between analyzer A and horizontal electrodes is 45° and (b): this angle is 0°.

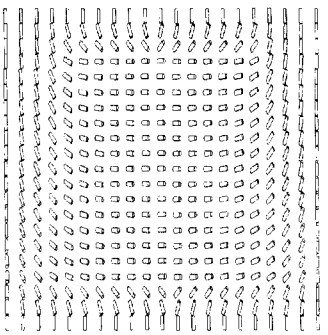

FIG. 8. Director distribution in the vertical y-z plane at $x=0$ for the case of two disclination line defects.

size R of the deformation can be taken as $R \approx \xi_3$, and r_c is the radius of the defect core (r_c is of the order of a molecular size, 2 nm).[20] Then, the core energy is $\pi m^2 K \alpha$, where α can vary between 0 and $\log R/r_c$.[22,23] The last term in Eq. (59) is the energy associated with two small wall defects which lie in the near-electrode layers and connect the defect lines to the electrode planes. Because both of these two numbers Δ and ξ_2 are inversely proportional to the electric field, this energy does not depend on voltage, and W_l increases with voltage very slowly (logarithmically). This means that at some critical voltage u_c there is a first order phase transition between the two director configurations. Taking into account that the horizontal length of the wall and lines is essentially the same and the height of the wall is approximately d, an equation for u_c results by equating the total energies associated with the wall and lines:

$$\frac{K_2 d}{\xi_2} \approx \frac{\pi K}{4}\left(\log\frac{\xi_3}{r_c}+\alpha\right)+\frac{K_2\Delta}{\xi_2}. \tag{60}$$

From Eq. (60) u_c is estimated to be between 20 and 40 V depending on the particular value of α.

It should also be noted that the medium outside the LC slab is usually a uniform glass plate with a dielectric constant ϵ_g (and not the vacuum). The simplest way to take this fact into account is to replace $\epsilon_\parallel \to \epsilon_\parallel/\epsilon_g$ in all the formulas (46)–(53) for the description the zero order solution without any changes in the description of the layers. As we found, this replacement, however, does not produce any significant and qualitative changes in the director distributions illustrated in the figures.

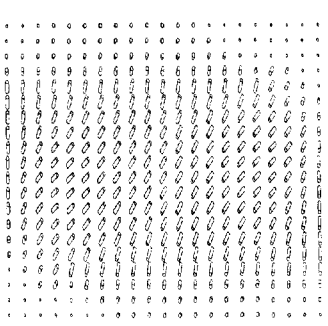

FIG. 9. Director distribution in the horizontal x-y plane at $z=0.4\,d$ for the case of two disclination line defects.

Finally, let us say a few words about possible corrections to the $\mathbf{n}_0(\mathbf{r})$ and $\mathbf{E}_0(\mathbf{r})$ distributions in the bulk. All corrections to the director distribution which come from taking into account the elastic energy along with the electric energy in the bulk are of orders δ, δ^2, ... and very small for $u \geqslant 10$ V. On the other hand, inside a layer $\mathbf{n}(\mathbf{r})$ can differ from $\mathbf{n}_0(\mathbf{r})$ significantly. Because a layer thickness is $\propto \delta^{1/2}$, it results in corrections of order $\delta^{1/2}$ to $\mathbf{E}_0$ and $\mathbf{n}_0$ in the bulk. It can be shown that the $\delta^{1/2}$ corrections due to the near-electrode layer can be found using relations $\Phi_{\rm vac}(x,y,d/2)=V(x,y)$ and

$$\Phi_{\rm LC}(x,y,d/2-\Delta)-V(x,y)=\int_{d/2-\Delta}^{d/2} dz E_z(x,y,z) \equiv \Delta\Phi_l(x,y) \tag{61}$$

instead of the continuity property of $\Phi_0(\mathbf{r})$ across the electrode plane, and by varying the following free energy functional

$$\mathrm{F}_{fl} \equiv \frac{1}{8\pi}\int d\rho\left[(\Phi_{\rm vac}\partial_z\Phi_{\rm vac})\big|_{z=d/2} - \epsilon_\parallel(\Phi_{\rm LC}\partial_z\Phi_{\rm LC})\big|_{z=d/2-\Delta}\right] \tag{62}$$

instead of Eq. (46). Using Eq. (23) one can calculate $\Delta\Phi_l(x,y)$ as a known function, assuming that $\theta(z)$ has already been found inside the layer. For example, using the simplest approximation of Eq. (27), it is possible to evaluate the integral in Eq. (61) analytically. Then, using the same representations of Eqs. (39), (40), (43), and (44), expanding $\Delta\Phi_l(x,y)$ in the double Fourier series and treating Eq. (62) exactly as before, one can find eventually those $\delta^{1/2}$ corrections. In a case when the wall layer is absent, corrections turned out to be small for $u \geqslant 10$ V. The reason for that is smallness of $\Delta\Phi_l$ (at average), which is of order of $\bar{E}_{0z}\Delta$ for a crude estimation. More detailed analysis of these corrections and generalization of the above consideration to include the wall layer as well as considering the possibility of weak homeotropic surface anchoring will be considered in future work.

V. CONCLUSION

The equations for describing the bright state of the liquid crystal cell having a homeotropic to multidomainlike transition were derived and solved to obtain the nonanalytical three dimensional structure of the electric field and director. The solution depends on the geometrical sizes of the cell, the physical parameters describing the liquid crystal (Frank constants and dielectric constants), and the voltage.

It was found that two different defect structures are possible for the director configuration: one corresponds to a wall defect and the other to two disclination lines. A first order phase transition between the two structures is predicted at a particular value of the voltage. The equation for determining this critical voltage was derived.

The solution provides a basis for calculation of the light transmission and for choosing the optimal conditions for operation of the display.

ACKNOWLEDGMENTS

This work was supported by the National Science Foundation under the Science and Technology Center ALCOM DMR89-20147. Helpful discussions with Professors P. J. Bos, J. Kelly and O. Lavrentovich are much appreciated. We would like also to acknowledge P. Watson, J. E. Anderson, and P. J. Bos for providing LC3Draw Liquid Crystal Director Visualization software.

[1] R. A. Sofer, J. Appl. Phys. **45**, 5466 (1974).
[2] R. Kiefer, B. Weber, F. Windscheid, and G. Baur, in *Proceedings of the 12th International Display Research Conference* (Society for Information Display and the Institute of Television Engineers of Japan, Hiroshima, 1992), p. 547.
[3] M. Oh-e and K. Kondo, Appl. Phys. Lett. **67**, 3895 (1995).
[4] M. Ohta, M. Oh-e, and K. Kondo, in *Proceedings of the 15th International Display Research Conference* (Society for Information Display and the Institute of Television Engineers of Japan, Hamamatsu, 1995), p. 577.
[5] K. Ohmuro, S. Kataoka, T. Sasaki, and Y. Koike, in *Digest of Technical papers of 1997 Society for Information Display International Symposium* (Society for Information Display, Boston, 1997), p. 845.
[6] S. H. Lee, J. G. You, H. J. Park, B. G. Rho, J. H. Lee, S. K. Kwon, and H. S. Park, in *Digest of Technical Papers of 1997 Society for Information Display International Symposium* (Society for Information Display, Boston, 1997), p. 675.
[7] P. L. Bos and J. A. Rahman, in *Digest of Technical Papers of 1993 Society for Information Display International Symposium* (Society for Information Display, Seattle, 1993), p. 273.
[8] Y. Yamaguchi, T. Miyashita, and Y. Uchida, in *Digest of Technical Papers of 1993 Society for Information Display International Symposium* (Society for Information Display, Seattle, 1993), p. 277.
[9] S. H. Lee, J. G. You, H. Y. Kim, B. G. Rho, S. K. Kown, H. S. Park, H. G. Galabova, and D. W. Allender, in *Digest of Technical Papers of 1997 Society for Information Display International Symposium* (Society for Information Display, Boston, 1997), p. 735.
[10] S. H. Lee, H. Y. Kim, H. G. Galabova, and D. W. Allender, Appl. Phys. Lett. **72**, 858 (1997).
[11] S. H. Lee, H. Y. Kim, I. C. Park, Y. H. Lee, B. G. Rho, J. S. Park, and H. S. Park, in *The 1st Korean Symposium on Information Display* (Korea Society for Information Display, Seoul, 1997), p. 23.
[12] S. H. Lee, H. Y. Kim, I. C. Park, B. G. Rho, J. S. Park, H. S. Park, and C. H. Lee, Appl. Phys. Lett. **71**, 2851 (1997).
[13] S. H. Lee, H. Y. Kim, T. K. Jung, I. C. Park, Y. H. Lee, B. G. Rho, J. S. Park, and H. S. Park, in *Proceedings of the 4th International Display Workshops* (Society for Information Display and the Institute of Television Engineers of Japan, Nagoya, 1997), p. 97.
[14] J. Hirata, Y. Hisatake, M. Ishikawa, M. Shoji, Y. Tanaka, H. Hatoh, in *Digest of Technical Papers of 1993 Society for Information Display International Symposium* (Society for Information Display, Seattle, 1993), p. 561.
[15] M. F. Schiekel and K. Fahrenschon, Appl. Phys. Lett. **19**, 391 (1971).
[16] K. H. Kim, S. B. Park, J. U. Shim, J. Chen, and J. H. Souk, in *Proceedings of the 4th International Display Workshops* (Society for Information Display and the Institute of Television Engineers of Japan, Nagoya, 1997), p. 175.
[17] S. H. Lee, H. Y. Kim, T. K. Jung, I. C. Park, Y. H. Lee, B. G. Rho, J. S. Park, and H. S. Park, in *Proceedings of the 4th International Display Workshops* (Society for Information Display and the Institute of Television Engineers of Japan, Nagoya, 1997), p. 9.
[18] W. Liu, J. Kelly, and J. Chen, in *Digest of Technical Papers of 1998 Society for Information Display International Symposium* (Society for Information Display, San Jose, 1998), p. 319.
[19] S. H. Lee, H. Y. Kim, Y. H. Lee, I. C. Park, B. G. Rho, H. G. Galabova, and D. W. Allender, Appl. Phys. Lett. **73**, 470 (1997).
[20] P. G. de Gennes and J. Prost, *The Physics of Liquid Crystals* (Oxford Science, New York, 1993).
[21] J. D. Jackson, *Classical Electrodynamics*, 2nd ed. (Wiley, New York, 1978).
[22] M. V. Kurik and O. D. Lavrentovich, Sov. Phys. Usp. **31**, 196 (1988).
[23] I. F. Lyuksyutov, Sov. Phys. JETP **48**, 178 (1978).